arXiv:1512.06930v3 [cond-mat.mtrl-sci] 24 Feb 2016

Accurate energy bands calculated by the hybrid quasiparticle self-consistent *GW* method implemented in the ecalj package

Daiki Deguchi and Kazunori Sato
Division of Materials and Manufacturing Science, Graduate School of Engineering, Osaka University, Suita, Osaka 565-0871, Japan

Hiori Kino
National Institute for Materials Science, Tsukuba, Ibaraki 305-0047, Japan

Takao Kotani
Department of Applied Mathematics and Physics, Tottori University, Tottori 680-8552, Japan

We have recently implemented a new version of the quasiparticle self-consistent *GW* (QSGW) method in the ecalj package released at http://github.com/tkotani/ecalj. Since the new version of the ecalj package is numerically stable and more accurate than the previous versions, we can perform calculations easily without being bothered with tuning input parameters. Here we examine its ability to describe energy band properties, *e.g.*, band-gap energy, eigenvalues at special points, and effective mass, for a variety of semiconductors and insulators. We treat C, Si, Ge, Sn, SiC (in 2H, 3C, and 4H structures), (Al, Ga, In)×(N, P, As, Sb), (Zn, Cd, Mg)×(O, S, Se, Te), SiO_2, HfO_2, ZrO_2, $SrTiO_3$, PbS, PbTe, MnO, NiO, and HgO. We propose that a hybrid QSGW method, where we mix 80% of QSGW and 20% of LDA, gives universally good agreement with experiments for these materials.

PACS numbers: 71.15.Ap, 71.20.Nr, 31.15.xm

I. INTRODUCTION

The quasiparticle self-consistent *GW* (QSGW) method is the best available method for finding a static one-body Hamiltonian H^0 that describes a system on the basis of the optimum independent-particle [or the quasiparticle (QP)] picture [1–7]. QSGW considers for an optimum division of the full many-body Hamiltonian H into $H = H^0+(H-H^0)$, by choosing H^0 so as to minimize the perturbative corrections caused by $(H - H^0)$ to the QPs described by H^0. That is, we perform a self-consistent calculation until the correction is minimized. Note that $(H-H^0)$ should contain not only a bare Coulomb interaction but also a quadratic term, which is missing in usual model Hamiltonians. In the QSGW methodm, we evaluate $(H-H^0)$ in the *GW* approximation; therefore, in the determination of H^0, charge fluctuations (not only local fluctuations but also plasmons) are taken into account self-consistently within the random phase approximation (RPA). We determine H^0, the self-energy $\Sigma(\mathbf{r}, \mathbf{r}', \omega)$, and the effective screened Coulomb interaction $W(\mathbf{r}, \mathbf{r}', \omega)$ simultaneously when we attain self-consistency in QSGW.

Kotani and his collaborators developed an all-electron *GW* method based on the full-potential linear muffin-tin orbital (FPLMTO) method [8] to perform QSGW calculations [1, 3]. We call this method FPLMTO-QSGW. FPLMTO-QSGW was applied to a wide range of materials and proved its potential to go beyond the abilities of current first-principles methods based on the density functional theory. [3, 7]. However, mainly because of the difficulty in the usage of FPLMTO, it is too complicated to apply FPLMTO-QSGW to a wide variety of materials. The main reason for this is that FPLMTO uses only atom-centered localized orbitals, Muffin-tin orbitals (MTOs), as a basis set to expand eigenfunctions. Choosing parameters specifying MTOs is not straightforward and requires fine tunings and repeated tests to perform reliable calculations. In addition, the offset-Γ method for the Brillouin zone (BZ) integration is slightly problematic in treating anisotropic systems.

To avoid these problems, Kotani and coworkers have developed a new method of implementing the QSGW method based on the linearized augmented plane-wave and muffin-tin orbital method (PMT method), which employs augmented plane wave (APW) and MTO basis sets [5, 9]. The PMT method is a unique mixed basis method that uses two types of augmented waves [9–11]. We call this new implementation of QSGW as PMT-QSGW and the package is open for public use as the ecalj package, which is available at https://github.com/tkotani/ecalj/ [12]. In this paper, we present practical applications of PMT-QSGW with the ecalj package to a variety of materials. The present calculation results have not been presented yet, although PMT-QSGW with the ecalj package was already used in the preceding studies [13–18] and the minimum examination of PMT-QSGW was reported in Ref. 5.

The purpose of the present study is twofold. On one hand, we show how accurately PMT-QSGW describes the band structure of semiconductors and insulators. The first-principles calculations based on the local density approximation (LDA) are now frequently used to explain material properties, but owing to its deficiency in the prediction of band properties, such as energy gap and effective mass, the application range of the LDA is somewhat limited. Obviously, we cannot directly use the LDA

to propose new photovoltaic or photocatalytic materials. Considering that the computational method becomes continuously important for exploring and fabricating new functional materials, it is important to show the reliability of the most advanced electronic structure theory, the so-called 'beyond LDA' theory such as QSGW, and encourage the first-principles calculations as a standard tool for designing new functional materials.

The other purpose of the present study is to demonstrate the usability of the ecalj package. Recently, the first-principles calculations have been used by both theoretical researchers and experimentalists for practical applications. In such a case, all users of the first-principles package are not always professionals. The ecalj package is designed so that all the calculations are performed essentially in its default settings; therefore, the users are not required to set the parameters that control the accuracy of the calculations. We only need to prepare information of crystal structures with a very limited number of inputs. By following the procedure described in Appendix, the users of the ecalj package can reproduce the results presented in this paper and actually observe the numerical stability and reliability of the ecalj package; thus the present paper serves a reference of standard calculation results.

After the minimum explanation of PMT-QSGW in the next section, we show the calculated band gaps. Then, we show the band properties and effective mass of materials with zincblende structures. Finally, we give a summary and possible expectations for the PMT-QSGW in the ecalj package. We would conclude that the PMT-QSGW in the ecalj package can be a useful tool for investigating problems not treated within the other standard electronic structure theories such as the LDA and hybrid methods. In Appendix, we show how to reproduce our results with the `ecalj` package.

II. METHOD

In this study, we apply the QSGW method implemented in the `ecalj` package to several materials. Readers are referred to Ref. 5 for details on the theory and implementation of the QSGW method. In this section, we give a minimum explanation of the QSGW method.

In the LDA, we use $V^{\rm xc}_{\rm LDA}(\mathbf{r})$ calculated from the electron density. This is calculated from a one-body Hamiltonian H^0. In contrast, we calculate $\Sigma(\mathbf{r},\mathbf{r}',\omega)$ from eigenfunctions and eigenvalues calculated from H^0. Then, we can obtain the static but nonlocal exchange-correlation potential in QSGW $V^{\rm xc}_{\rm QSGW}(\mathbf{r},\mathbf{r}')$, whose matrix elements are given as

$$V^{\rm xc}_{\rm QSGW} = \frac{1}{2}\sum_{ij} |\psi_i\rangle \left\{ {\rm Re}[\Sigma(\varepsilon_i)]_{ij} + {\rm Re}[\Sigma(\varepsilon_j)]_{ij} \right\} \langle\psi_j|, \tag{1}$$

where ε_i and $|\psi_i\rangle$ are the eigenvalues and eigenfunctions of H_0, respectively, and $\Sigma_{ij}(\omega) = \langle\psi_i|\Sigma(\omega)|\psi_j\rangle = \int d^3r \int d^3r' \psi^*_i(\mathbf{r})\Sigma(\mathbf{r},\mathbf{r}',\omega)\psi_j(\mathbf{r}')$. ${\rm Re}[\Sigma(\varepsilon)]$ is the real part of the self-energy, which assures the Hermiteness of the Hamiltonian [1, 3]. With this $V^{\rm xc}_{\rm QSGW}$, we can give a new static one-body Hamiltonian H^0 (by keeping $V^{\rm xc}_{\rm QSGW}$ instead of using $V^{\rm xc}_{\rm LDA}(\mathbf{r})$, we run a self-consistent calculation; then, the Hartree potential is also updated since the electron density is updated). Thus, we can perform the above procedure repeatedly until H^0 is converged. Simple semiconductors require about five iterations to achieve the convergence of eigenvalues within $\lesssim 0.01$ eV. More iterations are required for materials such as antiferromagnetic NiO and MnO. We should emphasize the importance of off-diagonal elements of Eq. (1) in resolving band entanglement, *e.g.*, in Ge [36]. In such a case, even for simple semiconductors such as Ge, we need fifteen iterations to obtain a well-converged band-gap energy.

Generally, the QSGW method systematically overestimates the band-gap energy [2, 3]. As suggested in Ref. 2, this can be due to the too small screening effect in the RPA, which neglects electron-hole correlations in the appropriate polarization function [4], and/or the screening effect of phonons suggested by Botti and Marques [37]. Thus, it must be preferable to use the above-mentioned methods to remedy the overestimation from the view point of physics; however, these methods can be computationally very demanding. Instead, in this study, we use an empirical procedure, a hybrid QSGW method introduced in Ref. 38. That is, we use

$$V^{\rm xc} = (1-\alpha)V^{\rm xc}_{\rm QSGW} + \alpha V^{\rm xc}_{\rm LDA}, \tag{2}$$

where we assume $\alpha = 0.2$, that is, 80% QSGW plus 20 % LDA in the calculations presented in this paper. We call this method QSGW80. In this method, we use the $V^{\rm xc}$ of Eq. (2) during the self-consistent cycle of QSGW. In this study, we also tested 'perturbative' QSGW80, that is, we used the $V^{\rm xc}$ of Eq. (2) after we obtained the self-consistent QSGW results of $\alpha = 0$. We call this 'perturbative' QSGW80 'non-self-consistent QSGW80', abbreviate as QSGW80(NoSC) in the following. This non-self-consistent procedure was previously used in Ref. 38. In Sect. III, we note that QSGW80 works reasonably well for a wide range of materials. This QSGW80 can be a simple solution to treat interfaces or superlattices such as CdSe/CdS [39], as long as both materials are described well with the same α.

Spin-orbit coupling (SO) is essential for the correct prediction of effective mass and band-gap energy. Considering the smallness of the effects of SO on the systems treated here, we can include SO as a perturbation after the scalar-relativistic self-consistent QSGW calculations.

III. RESULTS

We calculate the properties of the materials shown in Table I. The crystal structures and lattice constants of

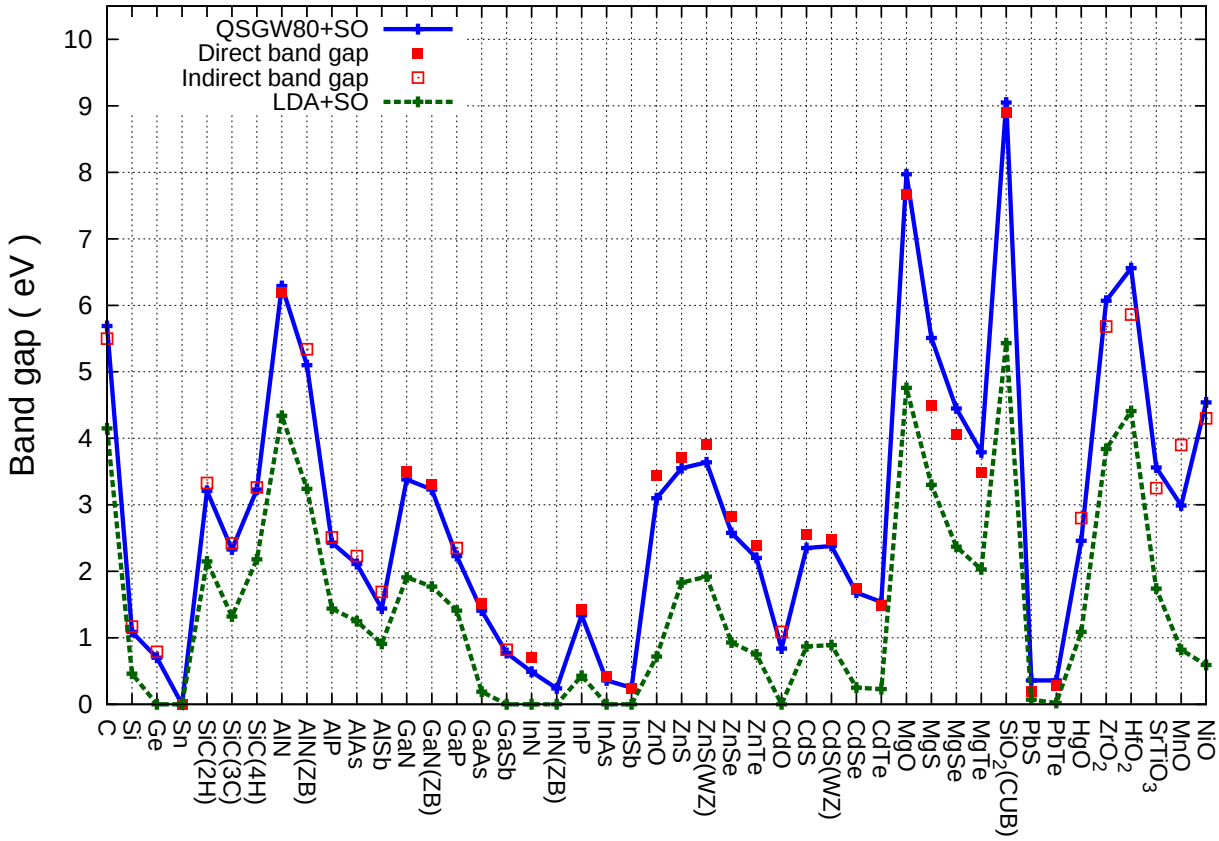

FIG. 1: Band-gap energies calculated by using QSGW80+SO (blue solid line) and LDA+SO (green dotted line), together with experimental values (solid squares: direct band gap, open squares: indirect band gap). Respective values are shown in Table II.

the materials are taken from experimental values. In addition to the fundamental IV, III-V, and II-VI semiconductors, we also include some important materials such as polytypes of SiC, Mg compounds, Pb compounds, and some oxides such as cubic SiO_2, HfO_2. We assume paramagnetic states except MnO and NiO, which exhibit a type II anti-ferromagnetic order [21]. For some materials such as AlN, we treat two structures, both with zincblende (ZB) and wurtzite (WZ) structures.

As shown in Table I, the number of $\mathbf{k}$ points in the 1st Brillouin zone (BZ) for the calculations of self-energy are $6\times6\times6$ for the zincblende structure in which two atoms are in the primitive cell. For the other structures, we reduce the number so as to keep the number of $\mathbf{k}$ points per atom almost the same, *e.g.*, we use $6\times6\times3$ for the wurtzite structure.

In the ecalj package, we use an interpolation technique for $V^{\rm xc}_{\rm QSGW}$ in the entire BZ [5]. This interpolation allows us to use a large number of $\mathbf{k}$ points in the step for determining H^0 for the given $V^{\rm xc}_{\rm QSGW}$. $V^{\rm xc}_{\rm QSGW}$ is calculated for the number of $\mathbf{k}$ points shown in Table I.

From the results of convergence check as shown in Ref. 5, we infer that numerical errors can be ~ 0.1 eV owing to the settings of parameters in the calculations. The number of MTOs per atom was $\sim$30, and it depends on atomic species. The cutoff energy of APWs is 3 Ry = 40.8 eV, which is good enough to reproduce energy bands without empty spheres [5].

A. Minimum band gap

The calculated minimum band-gap energies are shown in Table II. The label "+SO" means that the SO coupling was added after the convergence of the QSGW iteration. The label "QSGW80" means the hybrid calculation with $\alpha = 0.2$ in Eq. (2), that is, 80% of QSGW plus 20% of LDA. We observe that the normal QSGW with SO, *i.e.*, QSGW+SO, systematically overestimates the band-gap energy in comparison with experimental values. This overestimation was already observed in FPLMTO-QSGW [2, 3]. In contrast, we observe that QSGW80+SO shows a much better agreement with experiments systematically. In Fig. 1, we plot the QSGW80+SO values given in Table II, together with experimental values.

For most of the semiconductors shown in Table II, the deviations of the theoretical predictions from the experimental values are as large as $\sim$ 0.1 eV. This is in the

numerical uncertainty range of our implementation. In some cases, error can be slightly larger. For example, the calculated energy gap of InN(WZ) is 0.49 eV, which is 0.21 eV smaller than the experimental value of 0.7 eV. As for ZnO, the calculated value of 3.44 eV is 0.34 eV away from the experimental one of 3.10 eV. This is a case where the calculated band gap is largely affected by α since the LDA value is very small. For practical application to semiconductors, we need to take into consideration the accuracy shown in Table II. On the other hand, we should note that the experimental error bar of band gaps of materials (especially oxides) may not be sufficiently small, for example, the energy gap of MnO is 3.9 ± 0.4 eV.

In QSGW80(NoSC)+SO, we use Eq. (2) after we obtain the self-consistent $V^{\rm xc}_{\rm QSGW}$ with $\alpha = 0$ (usual QSGW). The difference from QSGW80+SO is not very large except in cases such as NiO, where QSGW80(NoSC)+SO gives 5.00 eV and QSGW80+SO gives 4.54 eV. This difference is due to the localized 3d electrons on cation sites. One may think that the large difference is due to the existence of the localized 3d orbital near the Fermi level, but it is not true because the energy gaps of 3.56 and 3.54 eV are obtained for $SrTiO_3$, electronic state of which is close to that of NiO apart from its magnetic nature. We can not discuss it further because we do not have enough data to investigate its origin. We observe smaller but slightly different values even in ZnO (3.10 and 3.26 eV).

We can observe the degree of the effect of SO as the difference between, *e.g.*, QSGW and QSGW+SO. As we see, materials including heavier atoms (especially anion) show larger SO effects. The difference between QSGW and QSGW+SO is very similar to that between QSGW80 and QSGW80+SO. This justifies our perturbative procedure for the SO coupling.

The label "QSGW1shot" means the 1shot *GW* calculation from the LDA result and the diagonalization including the off-diagonal elements of $V^{\rm xc}_{\rm QSGW}$ in Eq. (1). Thus, we can solve the entanglement problem. This is why our calculation gives the band gap for Ge, where the usual one-shot *GW* (eigenvalue shift only) cannot give the band gap [36]. In some cases, QSGW1shot can be useful from the view point of computational speed. QSGW1shot can be used as a practical tool since it can give a reasonable agreement with experiments for many semiconductors (To compare the calculated values with experimental values, we need to add the SO effect, which can be taken as the difference between QSGW80 and QSGW80+SO), although it is not applicable to materials such as NiO.

B. Band property of ZB-type semiconductors

We sometimes need quasi-particle energies at specific $\mathbf{k}$ points in BZ, for example, when we observe optical responses, which contain both direct and indirect transitions, or when we need to consider intervalley transitions. Here, we show the eigenvalues instead of band plots (see Appendix about how to show band plots).

In Table III, we show the eigenvalues, which can be interpreted as quasi-particle energies, at the Γ, X, and L points for five selected ZB materials. These values can be compared with those calculated in the hybrid functional HSE06 [40–42]. We can consider that QSGW80+SO shows good agreement with experiments. However, we also see its limitations of accuracy. For example, L^c_6 and Γ^c_6 for InP by QSGW80+SO are 2.18 and 1.34 eV, respectively. They are slightly different from the experimental values of 2.01 (L^c_6) and 1.42 (Γ^c_6) eV. The difference is slightly larger than the agreement of the band gap itself [1.34 eV (QSGW80+SO) and 1.42 eV (experiment) at the Γ point]. Thus, care should be taken about this level of error when we apply QSGW80+SO to materials. However, we simultaneously need to note the accuracy of experimental data shown in Table III. These data are mostly estimated by optical experiments, where we need to remove excitonic effects theoretically from the raw experimental data based on some simple assumptions. Therefore, the difference between QSGW80+SO and HSE06 could be within the experimental error range.

HSE06 values, taken from Ref. 40, also give good agreement with experimental values. HSE06 uses GGA, but corrects a short-range exchange part with the Hartree-Fock exchange term. Since the Hartree-Fock method can give very large band gaps, results can be strongly affected by the hybridization ratio. This is in contrast to QSGW80 where we only hybridized 20% of LDA so as to correct the small error of QSGW. One interesting observation is that HSE06 and QSGW80+SO give similar tendencies as for differences from experimental values. For example, the valence band width X^v_7 values of InP are -2.49 and -2.52 eV for QSGW80+SO and HSE06, respectively.

C. Effective mass of ZB-type semiconductors

Effective mass plays a key role in the evaluation of transport properties and eigenvalues in quantum well structures and so on. It is straightforward to calculate the effective mass in QSGW in the ecalj package since we have interpolation procedure in the entire BZ; namely, without any extra techniques such as Wannier interpolation, we can plot the band structure. We show the calculated effective mass along the [100] direction for ZB in Table IV (the effective masses along other directions are complicated [38]). As discussed in Ref. 40, the improvement of the prediction of the band-gap energy is essential for the correct prediction of the effective mass.

In Fig. 2, we illustrate how to calculate the effective masses for GaAs. To obtain effective masses along the [100] direction, we first calculate eigenvalues (quasiparticle energies) along the [100] direction on a very dense $\mathbf{k}$ mesh. Then, for example, in the case of the electron

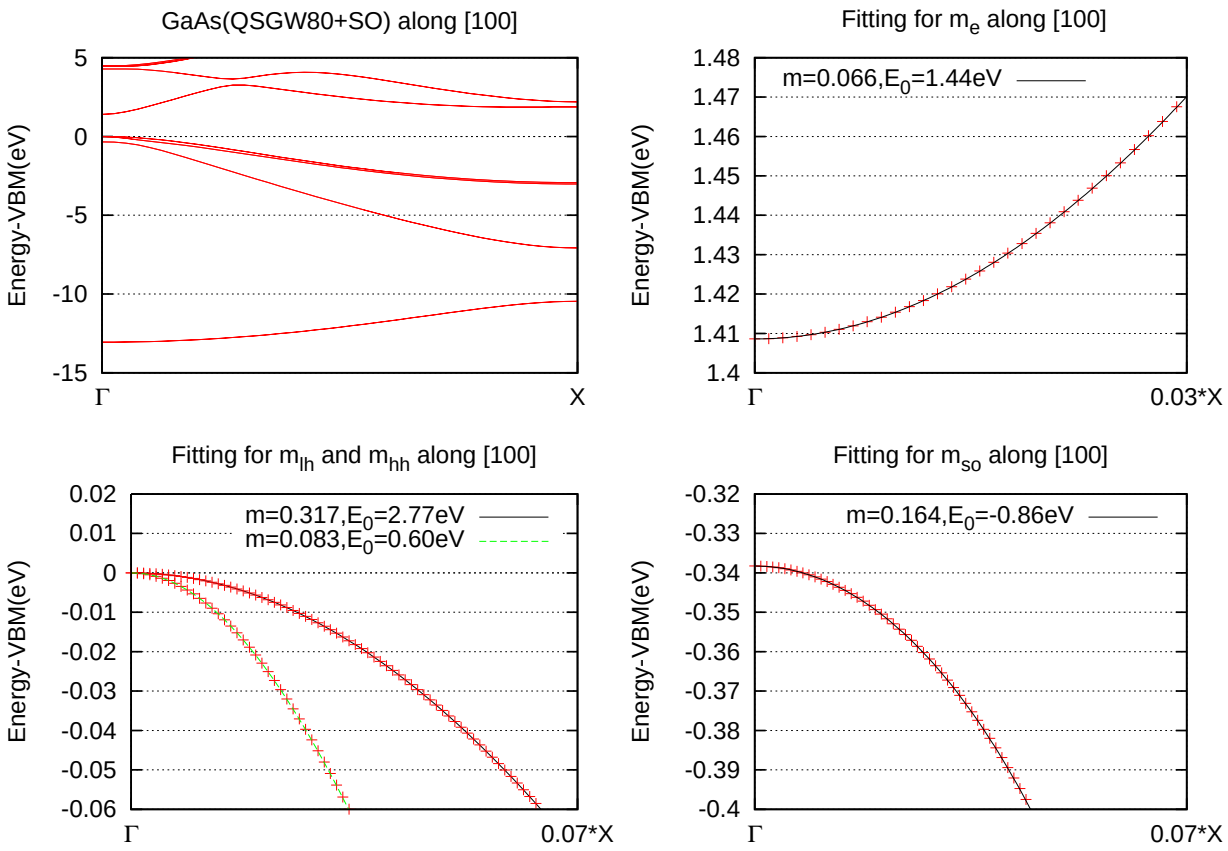

FIG. 2: Illustration about how to calculate effective masses for GaAs. The fitting window is between 0.01 and 0.05 eV for electrons (between -0.01 and -0.05 eV for holes) relative to the energy at the Γ point. We use the fitting formula [43], $E(|\mathbf{k}|)(1+E(|\mathbf{k}|)/E_0) = \hbar^2|\mathbf{k}|^2/(2m)$, and determine the effective mass m and correction E_0 to the parabolic behavior. See text.

mass $m_{\rm e}$, we consider the electron branch at the bottom of the conduction band. This branch of eigenvalues relative to the eigenvalue at the Γ point can be represented by $E^{\rm e}(|\mathbf{k}|)$ as a function of the length of $|\mathbf{k}|$. We now have $E^{\rm e}(|\mathbf{k}|)$ at dense $|\mathbf{k}|$ points along the [100] direction. Then, we perform a least square fitting for $E^{\rm e}(|\mathbf{k}|)$ in the energy window between 0.01 and 0.05 eV (or between -0.01 and -0.05 eV for holes). This range corresponds approximately to room temperature. Here, we use the fitting formula $E^{\rm e}(|\mathbf{k}|)(1+E^{\rm e}(|\mathbf{k}|)/E^{\rm e}_0) = \hbar^2|\mathbf{k}|^2/(2m_e)$, where the two parameters $E^{\rm e}_0$ and $m_{\rm e}$ (effective mass) are determined[43]. $E^{\rm e}_0$ is a parameter that modifies a parabolic behavior slightly. We apply the same procedure to other branches corresponding to the heavy hole mass $m_{\rm hh}$, the light hole mass $m_{\rm lh}$, and the mass for the split off band, $m_{\rm so}$. The calculated effective mass is summarized in Table IV.

As we see in Table IV, the agreement of theoretical effective masses with experiments ones is rather satisfactory, especially for the electron mass. If we like to treat the subband structure of a superlattice such as CdS/CdSe [39], we have to use a method that can reproduce not only the band gap and band offset, but also the effective mass. This is never expected in methods such as the LDA and the constant-shift procedure of the band gap (scissors operator procedure). In this sense, careful treatment may be necessary to compare experimental data with the results in Ref. 39.

IV. CONCLUSIONS

We have examined the ability of the QSGW method and the hybrid method QSGW80 implemented in the ecalj package to predict band properties such as band gap energy, eigenvalues at special points, and effective mass. The ecalj package can be used easily since the parameters for calculation are automatically set. With the hybrid scheme QSGW80, we can expect that the accuracy of band gaps can be ~ 0.1 eV for usual semiconductors. This level of accuracy is much higher than what we expect in the LDA. Considering the fact that QSGW can treat even metals accurately [3, 14, 15], we can expect that the QSGW or hybrid QSGWmethod can be appli-

cable to complex systems such as metal/semiconductor interfaces. However, it is necessary to know its limitations shown in this paper for such applications. In addition, note that QSGWcalculations are time-consuming, although we think there is so much room to improve the ecalj package for acceralating the calculations. For typical cases, the values of computational time per QSGW iteration by using one node of Xeon (it contains 24 cores, Hitachi HA8000-tc/HT210 in Kyushu university) are 2 min for C, 8 min for GaAs(ZB), 25 min for GaN(WZ), 36min for 4H-SiC(8 atoms/unitcell), and 150 min for HgO(8 atoms/cell). Computational time depends not only on the number of atoms per cell and the crystal symmetry but also on the atomic species. Usually, quasiparticle energies are converged within 0.01 eV after approximately five iterations.

Acknowledgments

This work was partly supported by the Advanced Low Carbon Technology Research and Development Program (ALCA) of Japan Science and Technology Agency (JST), and by Grants-in-Aid for Scientific Research 23104510 and 26286074. We also acknowledge the computing time provided by Computing System for Research in Kyushu University.

Appendix A: How to reproduce the calculations in this paper by using the ecalj package

The ecalj package is open for public use and all of the results presented in this paper can be reproduced by using the ecalj package by yourself. In this Appendix, the calculation procedure is briefly explained step by step. Owing to the limitation of space, we can show only the outline of the procedure. For detailed explanations and descriptions, visit https://github.com/tkotani/ecalj/[12].

1. **Installation of ecalj:** The ecalj package can be downloaded and installed from Ref. 12.The installer generates required binaries by using the Fortran compiler and performs minimum test calculations successively.

2. **Preparation of `ctrls` file:** To start a calculation of target material, we need to prepare a `ctrls.*` file, which contains information on the crystal structure. For the extension `*`, we usually use the name of the material, such as `gaas, zno`, and so on. The `ctrls` file is explained in detail at the link[12]. Instead of obtaining `ctrls.*` manually, you can use a converter, for example, `vasp2ctrl` is prepared for extracting information on the crystal structure from the POSCAR file for VASP (concerning VASP, see `https://www.vasp.at/`).

3. **Generating `ctrl` file:** From the `ctrls.*`, next we generate a `ctrl.*` file by using a python script, `ctrlgenM1.py`, included in the ecalj package. In addition to the information on the crystal structure, `ctrl.*` contains all of the parameters that control the calculations, such as information on MTOs, xc potential, number of k-points, relativistic treatment, and so on. In the generated `ctrl.*`, default settings are set to guarantee a reasonable calculation, but we need to edit them depending on the necessity. (With `ctrl.*`, we can perform DFT calculations.)

4. **Generating `GWinput`:** In addition to the `ctrl` file, we need one more input file, `GWinput`, which can be generated from `ctrls.*` by using a shell script (`mkGWIN_lmf2` also included in the `ecalj` package). `GWinput` contains settings for GW calculation.

   The input files used in this paper are basically produced from `ctrls.*` by following the above processes (2)-(4). To facilitate the reproduction of the present calculations by the users, we packed `ctrls.*`, `ctrl.*`, and `GWinput` for each material, which are available as supplementary data of this article at the web page[44].

5. **Performing** QSGW**:** With the two input files `ctrl.*` and `GWinput`, we can perform QSGW calculations by using a script `gwsc`. We set the number of iterations when we submit a job of `gwsc`. The output files of QSGW calculations are stored in `rst.*` and `sigm.*`. The outputs for the materials treated in this paper can be found also at the web page[44]. After we examine the convergence of eigenvalues, we proceed with post processing such as plotting the energy bands.

6. **Postprocessing:** Once the self-consistency is obtained, we can extract any material properties from the calculated electronic structure. How to do it is not trivial and an additional calculation or postprocessing is needed. As concerned with this paper, it is necessary to plot and fit energy bands for estimating the effective mass. As an example, the energy band of CdO is shown in Fig. 3 The energy-band plots for the other materials and fitting results can be found at the web page[44]. The files `syml.*`, which describes the k-point path for the band structure plot, are also packed. More details concerning the band plot can be found in the README given in the page[44].

[1] S. Faleev, M. van Schilfgaarde, and T. Kotani, Phys. Rev. Lett. **93**, 126406 (2004).

[2] M. van Schilfgaarde, T. Kotani, and S. Faleev, Phys. Rev.

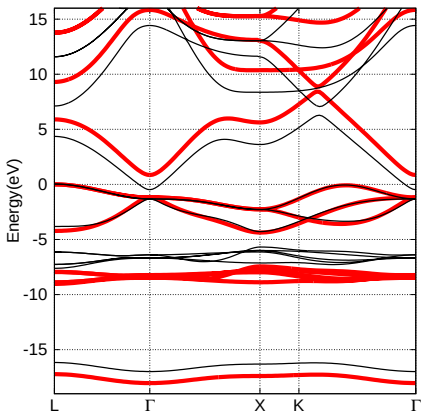

FIG. 3: Calculated band structure of CdO by using the LDA (thin black lines) and QSGW80 (thick red lines). The energy is relative to the valence band maximum.

Lett. **96**, 226402 (2006).

[3] T. Kotani and M. van Schilfgaarde, Phys. Rev. B **76**, 165106 (2007).

[4] M. Shishkin, M. Marsman, and G. Kresse, Phys. Rev. Lett. **99**, 246403 (2007).

[5] T. Kotani, J. Phys. Soc. Jpn. **83**, 094711 (2014).

[6] J. Klimeš, M. Kaltak, and G. Kresse, Phys. Rev. B **90**, 075125 (2014).

[7] F. Bruneval and M. Gatti, in *First Principles Approaches to Spectroscopic Properties of Complex Materials*, ed. C. Di Valentin, S. Botti, and M. Cococcioni (Springer, Heidelberg, 2014) Vol. 347, p. 99.

[8] M. Methfessel, M. V. Schilfgaarde, and R. A. Casali, in *Electronic Structure and Physical Properties of Solids: The Uses of the LMTO Method*, ed. H. Dreysse (Springer, Berlin, 2000) Lecture Notes in Physics Vol. 535.

[9] T. Kotani, H. Kino, and H. Akai, J. Phys. Soc. Jpn. **84**, 034702 (2015).

[10] T. Kotani and M. van Schilfgaarde, Phys. Rev. B **81**,125117 (2010).

[11] T. Kotani and H. Kino, J. Phys. Soc. Jpn. **82**, 124714 (2013).

[12] A first-principles electronic-structure suite based on the PMT method, `ecalj` package, is freely available at `https://github.com/tkotani/ecalj`. Its one-body part is developed on the basis of the LMTO part in the LMsuit package at `http://www.lmsuite.org/`.

[13] H. Ryee, S. Jang, H. Kino, T. Kotani, and M. Han, arXiv:1507.08746.

[14] S. W. Jang, T. Kotani, H. Kino, K. Kuroki, and M. J. Han, Sci. Rep. **5**,12050 (2015).

[15] M. J. Han, H. Kino, and T. Kotani, Phys. Rev. B **90**, 035127 (2014).

[16] H. Nagara, T. Ishikawa, and T. Kotani, High Pressure Res. **34**, 215 (2014).

[17] M. Geshi and T. Fukazawa, Physica B **411**, 154 (2013).

[18] A. Bakhtatou and A. Meddour, Phys. Status Solidi B (in press) [DOI: 10.1002/pssb.201552490].

[19] Crystallography Open Database (COD) [http://www.crystallography.net].

[20] P. Mélinon, *SiC Cage Like Based Materials* (InTech, Rijeka, 2011).

[21] K. Terakura, T. Oguchi, A. R. Williams, and J. Kübler, Phys. Rev. B **30**, 4734 (1984).

[22] L. W. S. H. Vosko, and M. Nusair, Can. J. Phys. **58**, 1200 (1980).

[23] O. Madelung, *Semiconductors: Data Handbook* (Springer, New York, 2004).

[24] W. J. Choyke, D. R. Hamilton, and L. Patrick, Phys. Rev. **133**, A1163 (1964).

[25] M. P. Thompson, G. W. Auner, T. S. Zheleva, K. A. Jones, S. J. Simko, and J. N. Hilfiker, J. Appl. Phys. **89**, 3331 (2001).

[26] G. Ramírez-Flores, H. Navarro-Contreras, A. Lastras-Martínez, R. C. Powell, and J. E. Greene, Phys. Rev. B **50**, 8433 (1994).

[27] V. Davydov, A. A. Klochikhin, R. P. Seisyan, V. V. Emtsev, S. V. Ivanov, F. Bechstedt, J. Furthmüller, H. Harima, A. V. Mudryi, J. Aderhold, O. Semchinova, and J. Graul, Phys. Status Solidi B **229**, R1 (2002).

[28] V. Davydov, A. A. Klochikhin, V. V. Emtsev, S. V. Ivanov, V. V. Vekshin, F. Bechstedt, J. Furthmüller, H. Harima, A. V. Mudryi, A. Hashimoto, A. Yamamoto, J. Aderhold, J. Graul, and E. E. Haller, Phys. Status Solidi B **230**, R4 (2002).

[29] O. Zakharov, A. Rubio, X. Blase, M. L. Cohen, and S. G. Louie, Phys. Rev. B **50**, 10780 (1994).

[30] S.-H. Wei and A. Zunger, Phys. Rev. B **55**, 13605 (1997).

[31] T. DiStefano and D. Eastman, Solid State Commun. **9**, 2259 (1971).

[32] S. Sayan, R. A. Bartynski, X. Zhao, E. P. Gusev, D. Vanderbilt, M. Croft, H. M. Banaszak-Holl, and E. Garfunkel, Phys. Status Solidi B **241**, 2246 (2004).

[33] S. Sayan, T. Emge, E. Garfunkel, X. Zhao, L. Wielunski, R. A. Bartynski, D. Vanderbilt, J. S. Suehle, S. Suzer, and M. Banaszak-Holl, J. Appl. Phys. **96**, 7485 (2004).

[34] K. van Benthem, C. Elsässer, and R. H. French, J. Appl. Phys. **90**, 6156 (2001).

[35] F. Tran and P. Blaha, Phys. Rev. Lett. **102**, 226401 (2009).

[36] M. van Schilfgaarde, T. Kotani, and S. Faleev, Phys. Rev. B **74**, 245125 (2006).

[37] S. Botti and M. A. L. Marques, Phys. Rev. Lett. **110**, 226404 (2013).

[38] A. N. Chantis, M. van Schilfgaarde, and T. Kotani, Phys. Rev. Lett. **96**, 086405 (2006).

[39] V. Kocevski, J. Rusz, O. Eriksson, and D. Sarma, Sci. Rep. **5**, 10865 (2015).

[40] Y.-S. Kim, M. Marsman, G. Kresse, F. Tran, and P. Blaha, Phys. Rev. B **82**, 205212 (2010).

[41] J. Heyd, G. E. Scuseria, and M. Ernzerhof, J. Chem. Phys. **118**, 8207 (2003).

[42] J. Heyd, G. E. Scuseria, and M. Ernzerhof, J. Chem. Phys. **124**, 219906 (2006).

[43] D. F. Helson, R. C. Miller, and D. A. Kleinman, Phys. Rev B **35**, 7770 (1987).

[44] Supplemental information is given at `https://github.com/tkotani/Supplement4deguchipaper.git`. It contains all information on how to perform calculations presented in this paper. Output files of QSGW calculations are also available with the band-structure plots and the fitting results for effective mass calculations.

TABLE I: Crystal structures used for the calculations in this paper and the number of **k** points for the self-energy calculations in the 1st Brillouin zone (see text). Labels mean as follows: COD: ID number of the crystal open database [19], DIA: diamond structure, HEX: hexagonal structure, ZB: zincblende structure, WZ: wurtzite structure, RS: rocksalt structure, CUB: cubic structure, MONO: monoclinic structure, TETRA: tetragonal structure, PERO: perovskite structure.

	Lattice constants (Å)	Crystal structure	Number of **k** for Σ
C	$a = 3.567$	DIA	6×6×6
Si	$a = 5.431$	DIA	6×6×6
Ge	$a = 5.646$	DIA	6×6×6
Sn	$a = 6.489$	DIA	6×6×6
SiC(2H)	$a = 3.076, c = 5.048$	HEX, COD9008875	6×6×3
SiC(3C)	$a = 4.348$	ZB, COD9008856	6×6×6
SiC(4H)	$a = 2.079, c = 10.07$	HEX, Ref. 20	4×4×2
AlN(WZ)	$a = 3.112, c = 4.982$	WZ	6×6×3
AlN(ZB)	$a = 4.38$	ZB	6×6×6
AlP	$a = 5.467$	ZB	6×6×6
AlAs	$a = 5.661$	ZB	6×6×6
AlSb	$a = 6.136$	ZB	6×6×6
GaN(WZ)	$a = 3.189, c = 5.189$	WZ	6×6×3
GaN(ZB)	$a = 4.50$	ZB	6×6×6
GaP	$a = 5.451$	ZB	6×6×6
GaAs	$a = 5.653$	ZB	6×6×6
GaSb	$a = 6.096$	ZB	6×6×6
InN(WZ)	$a = 3.545, c = 5.703$	WZ	6×6×3
InN(ZB)	$a = 4.98$	ZB	6×6×6
InP	$a = 5.870$	ZB	6×6×6
InAs	$a = 6.058$	ZB	6×6×6
InSb	$a = 6.479$	ZB	6×6×6
ZnO	$a = 3.254$	WZ	6×6×3
ZnS(ZB)	$a = 5.413$	ZB	6×6×6
ZnS(WZ)	$a = 3.82, c = 6.26$	WZ	6×6×3
ZnSe	$a = 5.667$	ZB	6×6×6
ZnTe	$a = 6.101$	ZB	6×6×6
CdO	$a = 4.72$	RS	6×6×6
CdS(ZB)	$a = 5.826$	ZB	6×6×6
CdS(WZ)	$a = 4.160, c = 6.756$	WZ	6×6×3
CdSe	$a = 6.054$	ZB	6×6×6
CdTe	$a = 6.482$	ZB	6×6×6
MgO	$a = 4.212$	RS	6×6×6
MgS	$a = 5.62$	ZB	6×6×6
MgSe	$a = 5.91$	ZB	6×6×6
MgTe	$a = 6.42$	ZB	6×6×6
PbS	$a = 5.936$	RS	6×6×6
PbTe	$a = 6.462$	RS	6×6×6
SiO_2c	$a = 7.165$	CUB	4×4×4
HgO	$a = 6.613, b = 5.521$	MONO	2×2×4
	$c = 3.522$	COD9012530	
ZrO_2	$a = 3.559, c = 5.111$	TETRA	4×4×2
HfO_2	$a = 3.545, c = 5.102$	TETRA	4×4×2
$SrTiO_3$	$a = 3.90$	PERO	4×4×4
MnO	$a = 4.445$	RS AF-II	4×4×4

TABLE II: Calculated minimum band-gap energies in eV by several calculation procedures. "+SO" means that the spin-orbit interaction is included after the self-consistency is obtained. QSGW80 means the calculation with 80% of QSGW together with 20% of LDA. QSGW80(NoSC) means that we use Eq. (2) when we make the band plot after the convergence of (pure) QSGW. QSGW1shot means one-shot QSGW (including off diagonal elements) from the LDA. In the LDA, we use the VWN exchange-correlation functional [22]. Expt. means experimental values, and D/I distinguishes the direct or indirect band gap. Experimental values are taken from Ref. 21 otherwise indicated. QSGW80+SO values together with LDA+SO and experimental ones are plotted in Fig. 1.

	LDA	LDA +SO	QSGW	QSGW +SO	QSGW 1shot	QSGW80	QSGW80 +SO	QSGW80 (NoSC)+SO	Expt.	D/I
C	4.16	4.15	6.11	6.11	5.88	5.69	5.69	5.71	5.50	I
Si	0.47	0.46	1.28	1.26	1.20	1.10	1.09	1.11	1.17	I
Ge	0.00	0.00	1.03	0.93	0.81	0.80	0.70	0.74	0.79	I
Sn	0.00	0.00	0.12	0.00	0.00	0.00	0.00	0.00	0	D
SiC(2H)	2.16	2.15	3.56	3.51	3.35	3.21	3.21	3.24	3.33	I
SiC(3C)	1.32	1.32	2.63	2.62	2.47	2.33	2.33	2.36	2.42	I
SiC(4H)	2.18	2.18	3.53	3.53	3.35	3.23	3.23	3.98	3.26[24]	I
AlN	4.34	4.34	6.91	6.91	6.41	6.30	6.29	6.40	6.19	D
AlN(ZB)	3.24	3.24	5.67	5.67	5.23	5.10	5.10	5.19	5.34[25]	I
AlP	1.46	1.44	2.74	2.72	2.56	2.45	2.43	2.47	2.51	I
AlAs	1.35	1.25	2.46	2.36	2.29	2.20	2.11	2.17	2.23	I
AlSb	1.13	0.91	1.80	1.59	1.69	1.65	1.44	1.49	1.69	I
GaN	1.91	1.91	3.84	3.83	3.45	3.38	3.38	3.45	3.50	D
GaN(ZB)	1.77	1.77	3.69	3.68	3.30	3.24	3.23	3.30	3.30[26]	D
GaP	1.44	1.41	2.49	2.46	2.31	2.25	2.23	2.26	2.35	I
GaAs	0.30	0.19	1.89	1.77	1.58	1.52	1.41	1.46	1.52	D
GaSb	0.00	0.00	1.20	0.99	1.01	0.99	0.77	0.79	0.82	I
InN	0.00	0.00	0.80	0.80	0.27	0.49	0.49	0.61	0.7[27, 28]	D
InN(ZB)	0.00	0.00	0.55	0.55	0.18	0.24	0.24	0.38	—	D
InP	0.46	0.43	1.65	1.62	1.40	1.37	1.34	1.38	1.42	D
InAs	0.00	0.00	0.80	0.68	0.47	0.48	0.36	0.43	0.42	D
InSb	0.00	0.00	0.77	0.54	0.51	0.49	0.25	0.29	0.24	D
ZnO	0.74	0.72	3.88	3.87	2.91	3.10	3.10	3.26	3.44	D
ZnS	1.86	1.83	4.12	4.10	3.62	3.57	3.55	3.65	3.71	D
ZnS(WZ)	1.94	1.92	4.21	4.18	3.70	3.66	3.64	3.74	3.91[29]	D
ZnSe	1.06	0.93	3.23	3.10	2.73	2.71	2.58	2.68	2.82	D
ZnTe	1.03	0.75	2.92	2.64	2.54	2.48	2.20	2.28	2.39	D
CdO	0.00	0.00	1.32	1.32	0.53	0.85	0.84	0.98	1.09	I
CdS	0.89	0.87	2.86	2.84	2.34	2.37	2.35	2.45	2.55[29]	D
CdS(WZ)	0.91	0.89	2.90	2.88	2.36	2.40	2.38	2.48	2.48	D
CdSe	0.37	0.25	2.28	2.16	1.71	1.81	1.68	1.78	1.74	D
CdTe	0.52	0.23	2.24	1.97	1.80	1.81	1.54	1.63	1.48	D
MgO	4.77	4.76	8.97	8.96	8.22	7.98	7.97	8.14	7.67	D
MgS	3.33	3.30	6.23	6.20	5.63	5.54	5.51	5.63	4.5	D
MgSe	2.50	2.37	5.24	5.11	4.67	4.58	4.45	4.59	4.05	D
MgTe	2.31	2.03	4.50	4.24	4.13	4.05	3.79	3.90	3.49	D
PbS	0.26	0.07	0.73	0.49	0.63	0.62	0.36	0.39	0.19[30]	D
PbTe	0.67	0.02	1.06	0.47	0.99	0.98	0.36	0.38	0.29[30]	D
SiO_2(CUB)	5.43	5.43	10.09	10.09	9.29	9.05	9.05	9.19	8.9[31]	D
HgO	1.11	1.09	2.89	2.89	2.53	2.49	2.46	2.54	2.8	I
ZrO_2	3.84	3.84	6.83	6.83	6.12	6.07	6.07	6.11	5.68[32]	I
HfO_2	4.42	4.41	7.29	7.25	6.63	6.57	6.56	6.61	5.86[33]	I
$SrTiO_3$	1.75	1.74	4.26	4.25	2.17	3.58	3.56	3.54	3.25[34]	I
MnO	0.89	0.82	3.94	3.82	2.10	3.10	2.99	3.29	3.9[35]	I
NiO	0.59	0.59	5.59	5.59	2.16	5.29	4.54	5.00	4.3[35]	I

TABLE III: Eigenvalues (in eV) relative to the top of the valence band at the Γ point for five selected zincblende materials. The values obtained by HSE06 [40] include the spin-orbit coupling. Experimental values are also taken from Ref. 40.

Material	E_g	QSGW +SO	QSGW80 +SO	HSE06	Expt.
InP	Γ_6^c	1.62	1.34	1.48	1.42
	X_6^c	2.48	2.26	2.35	2.38
	X_7^v	-2.54	-2.49	-2.52	-2.20
	L_6^c	2.46	2.18	2.25	2.01
	$L_{4,5}$	-1.05	-1.03	-1.03	-1.00
InAs	Γ_6^c	0.68	0.36	0.42	0.42
	X_6^c	2.09	1.88	1.98	1.90
	X_7^v	-2.65	-2.60	-2.64	-2.70
	L_6^c	1.74	1.46	1.53	—-
	$L_{4,5}$	-1.07	-1.05	-1.06	-0.90
InSb	Γ_6^c	0.54	0.25	0.28	0.24
	X_6^c	1.55	1.41	1.53	1.80
	X_7^v	-2.62	-2.57	-2.66	-2.24
	L_6^c	1.00	0.79	0.85	0.93
	$L_{4,5}$	-1.11	-1.09	-1.12	-1.05
GaAs	Γ_6^c	1.77	1.41	1.33	1.52
	X_6^c	2.09	1.88	1.96	2.18
	X_7^v	-2.99	-2.93	-2.99	-2.80
	L_6^c	1.98	1.69	1.67	1.85
	$L_{4,5}$	-1.25	-1.23	-1.25	-1.30
GaSb	Γ_6^c	1.09	0.77	0.72	0.81
	X_6^c	1.19	1.05	1.26	1.14
	X_7^v	-2.90	-2.86	-2.95	-2.72
	L_6^c	0.99	0.78	0.87	0.88
	$L_{4,5}$	-1.67	-1.26	-1.29	-1.32

TABLE IV: Effective mass ($m_{\rm e}$: electron, $m_{\rm lh}$: light hole, $m_{\rm hh}$: heavy hole, and $m_{\rm so}$: split off band) for zincblend materials along [100] direction calculated by QSGW80+SO. See text and Fig. 2 about how to calculate these values. We have poor fitting for $m_{\rm lh}$ and $m_{\rm so}$ for GaN(ZB) and InN(ZB); thus, no results are shown. Values in parentheses are experimental values taken from Ref. 40.

	$m_{\rm e}$	$m_{\rm lh}$	$m_{\rm hh}$	$m_{\rm so}$
GaN(ZB)	0.188	—-	0.807	—-
GaP	0.128	.159	0.369	0.231
GaAs	0.066	0.083	0.317	0.164
	(0.067)	(0.090)	(0.350)	(0.172)
GaSb	0.043	0.048	0.232	0.143
	(0.039)	(0.044)	(0.250)	(0.120)
InN(ZB)	0.024	—	1.022	—-
InP	0.079	0.101	0.412	0.173
	(0.080)	(0.121)	(0.531)	(0.210)
InAs	0.024	0.028	0.344	0.100
	(0.026)	(0.027)	(0.333)	(0.140)
InSb	0.017	0.019	0.251	0.126
	(0.014)	(0.015)	(0.263)	(0.110)
ZnS	0.186	0.252	0.643	0.376
ZnSe	0.128	0.175	0.542	0.313
ZnTe	0.112	0.135	0.395	0.286
CdS	0.152	0.200	0.698	0.331
CdSe	0.105	0.143	0.578	0.286
CdTe	0.093	0.114	0.420	0.285
MgS	0.248	0.409	1.261	0.634
MgSe	0.200	0.327	1.037	0.553
MgTe	0.174	0.258	0.732	0.495